

MambaVF: State Space Model for Efficient Video Fusion

Zixiang Zhao¹ Yukun Cui² Lilun Deng² Haowen Bai³ Haotong Qin¹ Tao Feng⁴ Konrad Schindler¹

Abstract

Video fusion is a fundamental technique in various video processing tasks. However, existing video fusion methods heavily rely on optical flow estimation and feature warping, resulting in severe computational overhead and limited scalability. This paper presents **MambaVF**, an efficient video fusion framework based on state space models (SSMs) that performs temporal modeling without explicit motion estimation. First, by reformulating video fusion as a sequential state update process, MambaVF captures long-range temporal dependencies with linear complexity while significantly reducing computation and memory costs. Second, MambaVF proposes a lightweight SSM-based fusion module that replaces conventional flow-guided alignment via a spatio-temporal bidirectional scanning mechanism. This module enables efficient information aggregation across frames. Extensive experiments across multiple benchmarks demonstrate that our MambaVF achieves state-of-the-art performance in multi-exposure, multi-focus, infrared-visible, and medical video fusion tasks. We highlight that MambaVF enjoys high efficiency, reducing up to 92.25% of parameters and 88.79% of computational FLOPs and a 2.1 \times speedup compared to existing methods. Project page: mambavf.github.io.

1. Introduction

Video fusion focuses on the joint exploitation of heterogeneous video sources, aiming to integrate complementary information from multiple sensors (*e.g.*, infrared-visible and medical MRI-CT) or vary acquisition conditions (*e.g.*, multi-exposure and multi-focus) into a unified video representation (Zhao et al., 2025). By enriching visual content with modality-specific characteristics while preserving consistency across frames, video fusion enhances scene inter-

¹ETH Zürich ²Xi'an Jiaotong University ³Nanyang Technological University ⁴Tsinghua University. Correspondence to: Yukun Cui <yukun.cui@hotmail.com>.

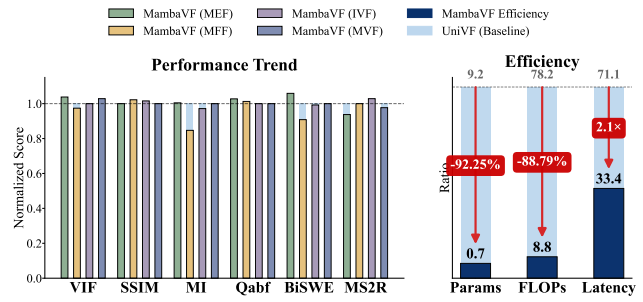


Figure 1. Compared with UniVF (Zhao et al., 2025), our MambaVF not only attains state-of-the-art performance on VF-Bench (Zhao et al., 2025), but also requires only 7.75% of the parameters and 11.21% of the FLOPs, while achieving a 2.1 \times speedup.

preability and robustness against adverse factors such as illumination variations and weather degradation (Zhao et al., 2023b; Liu et al., 2022; Zhang, 2021). It can also provide reliable and information-complete inputs for downstream tasks that need stable and continuous visual observations, including computational imaging (Chen et al., 2025), autonomous driving (Prakash et al., 2021), robotic perception (Li et al., 2023b), and clinical diagnosis (Li et al., 2023c) under complex environments.

The advanced video fusion methods always rely on optical flow estimation and explicit feature warping to enable multi-frame learning and temporal alignment. For example, UniVF (Zhao et al., 2025) is the most pioneering work to use these techniques in multi-frame learning, which achieves impressive video fusion performance across various fusion scenarios. However, the flow-based approach faces two fundamental bottlenecks. (i) *Computational inefficiency*: as illustrated in Fig. 2, optical flow estimation and warping-related operations are prohibitively expensive, accounting for over 78.09% of the total runtime, 91.94% of the parameters, and 79.85% of the FLOPs. (ii) *Sensitivity to accuracy*: the quality of fusion is strictly upper-bounded by the stability of flow estimation; any occlusion, fast motion, or illumination change that leads to flow inaccuracy will inevitably cause ghosting artifacts or blurring in the fused results. Moreover, abandoning optical flow in favor of global self-attention-based transformers to directly aggregate spatio-temporal information would incur an even higher computational burden. Because the quadratic complexity of full attention over spatial, temporal, and modality dimen-

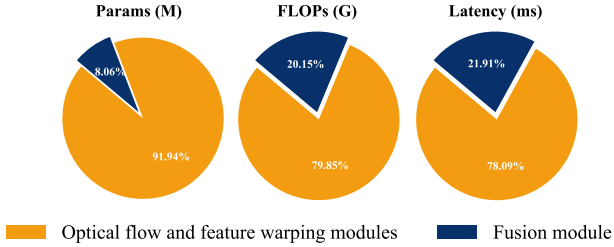


Figure 2. Parameter, FLOPs, and runtime contribution of optical flow and feature warping modules in UniVF (Zhao et al., 2025).

sions is extremely heavy, which renders such approaches impractical for long video sequences. These limitations significantly hinder the deployment of video fusion algorithms on resource-constrained edge devices, such as smartphones, drones, and wearable robots, which demand both high real-time performance and low power consumption.

Meanwhile, State Space Models (SSMs), particularly the Mamba architecture (Gu & Dao, 2024), have demonstrated extraordinary potential in modeling long-range dependencies with linear computational complexity. Unlike Transformers suffering from quadratic complexity relative to sequence length, Mamba’s efficient latent space update mechanism is inherently suited for video data, a domain characterized by high temporal redundancy and long-term correlations (Li et al., 2024; Argaw et al., 2025). More importantly, the hardware-aware design of Mamba allows for fine-grained feature extraction across both spatial and temporal dimensions without the need for explicit, computationally heavy alignment and warping modules based on optical flow.

Motivated by these insights, we propose **MambaVF**, a novel and efficient SSM-driven video fusion framework. MambaVF breaks the traditional practice that aligns optical flow explicitly. Instead, it leverages a hidden state transition mechanism to implicitly capture temporal dynamics within each source in a unified manner, while enabling effective cross-source interaction during the subsequent fusion stage. To further enhance the model’s ability to perceive complex video content, we introduce an innovative *spatio-temporal bidirectional* (STB) scanning mechanism. Different from standard 1D and 2D scanning, our STB approach performs a comprehensive traversal across spatial coordinates, temporal frames, and feature channels. This allows the model to prioritize salient textures and local structures in a spatio-temporal aware latent space, ensuring that the most informative features from multi-source inputs are preserved and fused with high fidelity.

The contributions of this work are summarized as follows:

- We propose MambaVF, the first video fusion framework based on State Space Models. By eliminating the

need for optical flow and feature warping, we provide a new, highly efficient paradigm for video fusion.

- We introduce a spatio-temporal bidirectional scanning mechanism in MambaVF, which enables the Mamba blocks to holistically understand video content across different dimensions.
- Extensive experiments on VF-Bench demonstrate that MambaVF achieves performance comparable to state-of-the-art methods. Remarkably, compared to the current leading baseline, our method requires only **7.75%** of the parameters and **11.21%** of the FLOPs, and achieves a **2.1x** speedup.

2. Related Work

Image and Video Fusion. Deep learning-based image fusion (Zhao et al., 2023b; Zhang, 2021) primarily divides into discriminative and generative paradigms. Discriminative methods (Xu et al., 2021; Zhao et al., 2022a; Li et al., 2023a; Zhao et al., 2022b) use CNNs (Prabhakar et al., 2017; Han et al., 2022; Gao et al., 2022; Bouzos et al., 2023; Guan et al., 2023; Deng et al., 2021) and Transformers (Qu et al., 2022; Guan et al., 2023) via model- or data-driven strategies (Xu et al., 2021; Zhao et al., 2022a; Li et al., 2023a; Zhao et al., 2022b; 2020; 2023b; Li & Wu, 2018). Generative approaches (Ma et al., 2019; Liu et al., 2022) treat fusion as distribution fitting, evolving from GANs (Ma et al., 2019; 2020) to Diffusion models (Chen et al., 2025; Zhao et al., 2023c), and recently to efficient one-step generation via Rectified Flow (Wang et al., 2025). To obtain more robust results, methods employ registration (Tang et al., 2025b; Wang et al., 2022a; Jiang et al., 2022; Xu et al., 2022b) for misalignment and combined restoration for complex degradations (Cao et al., 2025; Zhang et al., 2025). Concurrently, fusion is guided by downstream task feedback (Liu et al., 2025; Bai et al., 2025b; Zhong et al., 2025), cross-task synergy (Cheng et al., 2025; Xu et al., 2022a; Liang et al., 2022; Zhu et al., 2024b), and meta-learning (Bai et al., 2025c;a; Zhao et al., 2023a). Recently, vision-language priors (Zhao et al., 2024b) and text prompts (Zhang et al., 2024a) have emerged for interactive, controllable fusion.

Then, to enhance the understanding of dynamics, image fusion has been extended to the video domain. Tang et al. (2025a), Xie et al. (2024), and Gong et al. (2025) mainly focus on multi-modal scenarios. UniVF (Zhao et al., 2025) proposes a unified video fusion framework that provides a comprehensive multi-frame learning paradigm for multiple fusion tasks, including multi-exposure, multi-focus, infrared-visible, and medical video fusion. This framework standardizes the learning objective, datasets, and evaluation protocols across these diverse scenarios.

State Space Model in Computer Vision. Recently, State Space Models (SSMs) (Gu et al., 2021) have become a

hot topic for efficient sequence modeling. In particular, Mamba (Gu & Dao, 2024) has shown powerful performance in natural language processing by introducing a selective scan mechanism. Mamba demonstrates powerful capabilities in modeling long-range dependencies with linear computational complexity, bridging the gap between the efficiency of CNNs and the global receptive field of Transformers. Given the success of these efficient designs, a lot of studies have adapted 1D SSMs to 2D visual tasks. Architectures like Vim (Zhu et al., 2024a) and VMamba (Liu et al., 2024a) use bidirectional or cross-scanning strategies to process images in visual recognition. In low-level vision, MambaIR (Guo et al., 2024) utilizes SSMs to restore pixel-level image details. Furthermore, recent works like VideoMamba (Li et al., 2024), Vivim (Yang et al., 2025), Vamba (Ren et al., 2025) and Video Mamba Suite (Chen et al., 2026) have extended this to the spatiotemporal domain, providing an efficient way to maintain temporal consistency without heavy computational cost. Inspired by this, we aim to introduce the Mamba architecture to multi-source video fusion tasks, utilizing its efficient global modeling ability to handle cross-modal interactions and temporal evolution simultaneously.

3. MambaVF

In this section, we present the architecture of MambaVF, an efficient state space model for unified video fusion. We first provide an overview of the framework, followed by a detailed description of feature extraction, the *Spatio-Temporal Bidirectional (STB) Scanning* mechanism within the *Vision State Space (VSS)* blocks, and the reconstruction processes.

3.1. Overview

Given two synchronous multi-source video sequences $S_1, S_2 \in \mathbb{R}^{B \times T \times C \times H \times W}$, where B, T, C, H, W denotes the batch size, number of frames, channels, height, and width respectively, MambaVF aims to generate a fused video sequence that integrates complementary information without explicit motion estimation.

The overall pipeline consists of three main stages, which is illustrated in Fig. 3. First, the input videos are processed by a patch embedding layer to map the raw pixels into a latent embedding space. Second, a dual-stream Tri-Axis Mamba Encoder, consisting of multiple VSS blocks, extracts deep spatio-temporal features for each source independently. Third, the features from both streams are concatenated along the channel dimension and fed into a Mamba Decoder to reconstruct the final fused frames. Unlike previous flow-based methods, MambaVF maintains temporal consistency through the internal hidden states of the state space model.

3.2. Feature Extraction

Feature Embedding. MambaVF utilizes a dual-stream architecture to preserve the distinct characteristics of each source (*e.g.*, the thermal radiation in infrared and the texture details in visible videos). Each stream begins with a Tubelet Embedding layer:

$$E_S^1 = \text{Embedding}(S_1), \quad E_S^2 = \text{Embedding}(S_2). \quad (1)$$

This operation converts the video into a sequence of spatio-temporal tokens. These tokens are then passed through a series of VSS blocks. Each block contains a LayerNorm layer, the proposed STB-based selective scan module, and a residual connection. Since the model does not use computationally expensive self-attention, it maintains linear complexity with respect to the number of tokens.

Spatio-Temporal Bidirectional (STB) Scanning. The core of our MambaVF is the Spatio-Temporal Bidirectional (STB) scanning mechanism designed to capture the complex dependencies in video data. Standard 2D Mamba models typically use four-way scanning (diagonal directions) for images. However, video fusion requires modeling both instantaneous spatial textures and long-term temporal evolutions. Thus, we propose an 8-way scanning strategy to holistically perceive the video cube. A more intuitive visualization is provided in Fig. 3.

Let $x \in \mathbb{R}^{C \times T \times H \times W}$ denote the input spatio-temporal feature (*i.e.*, $\{E_S^1, E_S^2\}$). To comprehensively capture dynamics of the video cube, we rearrange the tokens into eight distinct scanning trajectories based on different priority axes:

1. *Spatial-Priority Scanning*: The trajectories are constructed by prioritizing spatial coverage within each temporal slice. Specifically, the scan follows a row-major order (traversing across width W then height H) and a column-major order (across H then W) for every frame. This strategy concentrates on extracting intra-frame structural correlations and local spatial textures.
2. *Temporal-Priority Scanning*: The sequence is formed by treating the temporal dimension T as the primary axis. In this mode, the model tracks the evolution of individual spatial coordinates (i, j) along the timeline before moving to the next pixel location. This pixel-wise temporal traversal is essential for the model to perceive motion trajectories and identify salient moving objects.
3. *Symmetrical Bidirectional Flipping*: For each of the four spatial and temporal priority paths described above, we also implement a reverse traversal. This bidirectional mechanism ensures that the state-space model can aggregate information from both preceding and succeeding contexts within the temporal window.

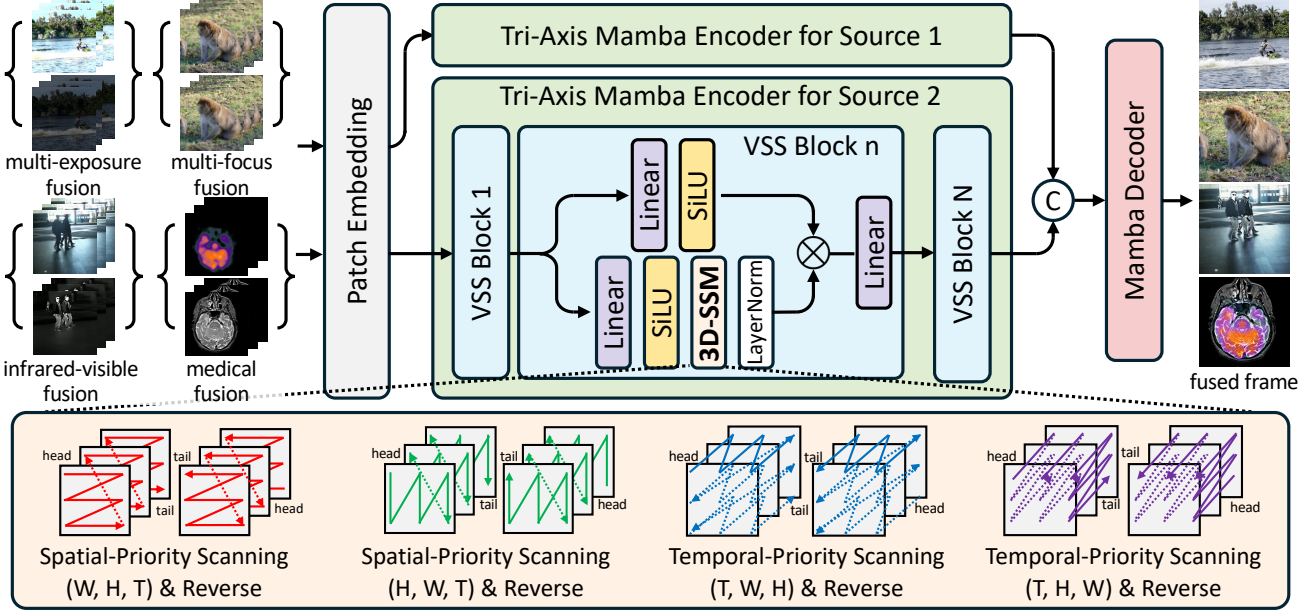


Figure 3. An overview of the proposed **MambaVF** architecture.

Each resulting sequence is processed by a selective scan operation. Discretized state space model is formulated as:

$$h_t = \bar{A}h_{t-1} + \bar{B}x_t, \quad y_t = Ch_t + Dx_t, \quad (2)$$

where the hidden state h_t functions as an implicit alignment bridge that synchronizes information across different frames. After the multi-path scanning, the 8 sequences are mapped back to their original spatio-temporal dimensions and integrated to form the enhanced feature representation.

3.3. Fusion and Reconstruction

After deep feature extraction, the features from the two streams F_1, F_2 are merged via channel-wise concatenation:

$$\begin{aligned} F_1 &= \text{STB}(E_S^1), \quad F_2 = \text{STB}(E_S^2), \\ F_{\text{fused}} &= \text{Concat}([F_1, F_2]). \end{aligned} \quad (3)$$

The fused features are subsequently processed by the Mamba Video Decoder. This module utilizes a sequence of VSS blocks to further characterize complex cross-modal dependencies within the latent space, followed by 2D Residual Blocks (He et al., 2016) to restore fine-grained textures and project the high-dimensional embeddings back to the pixel domain:

$$\hat{V} = \text{Decoder}(F_{\text{fused}}). \quad (4)$$

It is worth noting that, since the decoder is specifically optimized to reconstruct the central frame of the input window, it employs a 4-way spatial scanning strategy (*i.e.*, image-domain scanning) rather than the 8-way spatio-temporal

traversal. This design choice concentrates the state-space modeling on intra-frame structural refinement, ensuring high-fidelity spatial reconstruction for the target frame.

4. Experiments

We conduct a rigorous evaluation of MambaVF on the VF-Bench (Zhao et al., 2025) across four diverse scenarios: multi-exposure fusion (MEF), multi-focus fusion (MFF), infrared-visible fusion (IVF), and medical video fusion (MVF). The following sections detail our experimental configuration, performance comparisons, computational efficiency, and comprehensive ablation analysis.

4.1. Experimental Configuration

Loss Function. Following the optimization strategy in UniVF (Zhao et al., 2025), MambaVF is trained using a multi-term loss function that balances spatial, structural, and temporal fidelity:

$$\mathcal{L} = \mathcal{L}_{\text{spatial}} + \alpha_1 \mathcal{L}_{\text{grad}} + \alpha_2 \mathcal{L}_{\text{temp}}. \quad (5)$$

The weighting coefficients $\{\alpha_1, \alpha_2\}$ are task-specific: $\{10, 5\}$ for MEF, $\{1, 0.5\}$ for MFF, $\{5, 5\}$ for IVF, and $\{1, 1\}$ for MVF. The hyper-parameters for loss weights are adjusted according to the specific requirements of each fusion task to ensure stable convergence. The individual loss components are defined as follows:

(a) *Spatial Similarity* ($\mathcal{L}_{\text{spatial}}$): This term supervises the photometric distribution of the fused output. For IVF and MVF, we maximize intensity saliency: $\mathcal{L}_{\text{spatial}} = \frac{1}{HW} \|I_t^F -$

$\max(I_t^1, I_t^2)\|_1$. For MEF, it combines a mean intensity term $\mathcal{L}_{int} = \frac{1}{HW}\|I_t^F - \text{mean}(I_t^1, I_t^2)\|_1$ and the MEF-SSIM loss (Ma et al., 2015). For MFF, $\mathcal{L}_{spatial}$ is equivalent to $\mathcal{L}_{int} = \frac{1}{HW}\|I_t^F - \text{mean}(I_t^1, I_t^2)\|_1$.

(b) *Gradient Preservation* (\mathcal{L}_{grad}): To sharpen fused textures, we utilize a Sobel-based gradient loss: $\mathcal{L}_{grad} = \frac{1}{HW}\|\|\nabla I_t^F\| - \max(\|\nabla I_t^1\|, \|\nabla I_t^2\|)\|_1$, encouraging the retention of high-frequency structural details from both sources.

(c) *Temporal Consistency* (\mathcal{L}_{temp}): This term penalizes abrupt inter-frame intensity fluctuations, ensuring smooth photometric transitions without explicit motion compensation. For a detailed derivation of these objectives, please refer to Zhao et al. (2025).

Implementation Details. The MambaVF framework is implemented using PyTorch and trained on $4 \times$ NVIDIA GH200 GPUs. We utilize the Adam optimizer with an initial learning rate of 1×10^{-4} , which is gradually reduced through an exponential decay strategy over 20k iterations. The training process uses a batch size of 32 with gradient accumulation. Regarding the model architecture, MambaVF is configured with two encoders for different sources and a decoder, each composed of 3 VSS blocks with an embedding dimension of 32.

Evaluation Protocol. Following the evaluation protocol in VF-Bench (Zhao et al., 2025), our evaluation encompasses both spatial and temporal dimensions. For spatial quality, we employ *Visual Information Fidelity* (VIF), *Structural Similarity* (SSIM), *Mutual Information* (MI), and $Q^{AB/F}$. For temporal stability, we adopt the *Bi-Directional Self-Warping Error* (BiSWE) and *Motion Smoothness with Dual Reference Videos* (MS2R) to quantify flickering and motion artifacts. Higher values in spatial metrics and lower values in temporal metrics indicate superior fusion performance.

4.2. Video Fusion Experiments

We compare MambaVF with SOTA methods on four video fusion tasks to demonstrate its superior performance. In addition, qualitative video comparison results are provided in the supplementary material.

Multi-Exposure Video Fusion. MEF task requires the model to synthesize high-dynamic-range content from sequences with varying exposure levels. We compared MambaVF against SOTA methods including CUNet (Deng & Dragotti, 2020), HoLoCo (Liu et al., 2023), CRMEF (Liu et al., 2024b), TC-MoA (Zhu et al., 2024b), FILM (Zhao et al., 2024b), ReFusion (Bai et al., 2025c), and UniVF (Zhao et al., 2025). As illustrated in Fig. 4, MambaVF demonstrates a superior ability to recover details in both extremely dark and saturated regions. Our state-space-based approach models the temporal evolution of luminance implicitly. This leads to a more natural transition

of light and shadow, achieving higher VIF scores and significantly lower MS2R values in Tab. 1, proving that MambaVF can maintain high-fidelity textures while ensuring temporal alignment in dynamic lighting conditions.

Multi-Focus Video Fusion. In MFF, the objective is to integrate the focused regions from different focal planes into an all-in-focus video. We evaluated MambaVF against CUNet (Deng & Dragotti, 2020), RFL (Wang et al., 2022b), EPT (Wang et al., 2023), TC-MoA (Zhu et al., 2024b), FILM (Zhao et al., 2024b), ReFusion (Bai et al., 2025c), and UniVF (Zhao et al., 2025). MambaVF effectively addresses halo artifacts near the focus boundaries through its 8-way STB scanning mechanism, which captures the sharpness cues from both spatial and temporal perspectives. Our method accurately identifies the transition zones between focused and defocused areas, preserving sharp edges across the entire sequence. Fig. 5 and Tab. 1 on VF-Bench shows that MambaVF outperforms baseline models, particularly in scenes with complex depth-of-field changes where traditional image-based methods struggle to maintain boundary consistency.

Infrared-Visible Video Fusion. We compared our model with EMMA (Zhao et al., 2024a), TC-MoA (Zhu et al., 2024b), MRFS (Zhang et al., 2024b), FILM (Zhao et al., 2024b), ReFusion (Bai et al., 2025c), Text-DiFuse (Zhang et al., 2024a), DCEvo (Liu et al., 2025), TemCoCo (Gong et al., 2025), and UniVF (Zhao et al., 2025). MambaVF excels at preserving the high-contrast thermal signatures of infrared sources while retaining the rich environmental details of visible light. Qualitatively, our fused videos exhibit more prominent targets and clearer background structures in Fig. 6. Quantitatively, in Tab. 2, MambaVF achieves leading performance in VIF, SSIM and BiSWE, indicating that it successfully integrates the maximum amount of complementary information from both modalities while preserving video fluidity.

Medical Video Fusion. For Medical Video Fusion (MVF), we merged diverse modalities such as MRI, CT, and PET. Our evaluation included comparisons with EMMA (Zhao et al., 2024a), FILM (Zhao et al., 2024b), ReFusion (Bai et al., 2025c), Text-DiFuse (Zhang et al., 2024a), BSA-Fusion (Li et al., 2025), C2RF (Tang et al., 2025b), and UniVF (Zhao et al., 2025). MambaVF demonstrates exceptional performance in maintaining modality information. It preserves the fine-grained tissue textures of MRI images while successfully superimposing the functional intensity distributions from PET or SPECT. The results in Tab. 3 and Fig. 7 show that our model achieves the highest structural similarity scores and interframe similarity, effectively capturing the complex spatial relationships within medical volumes.

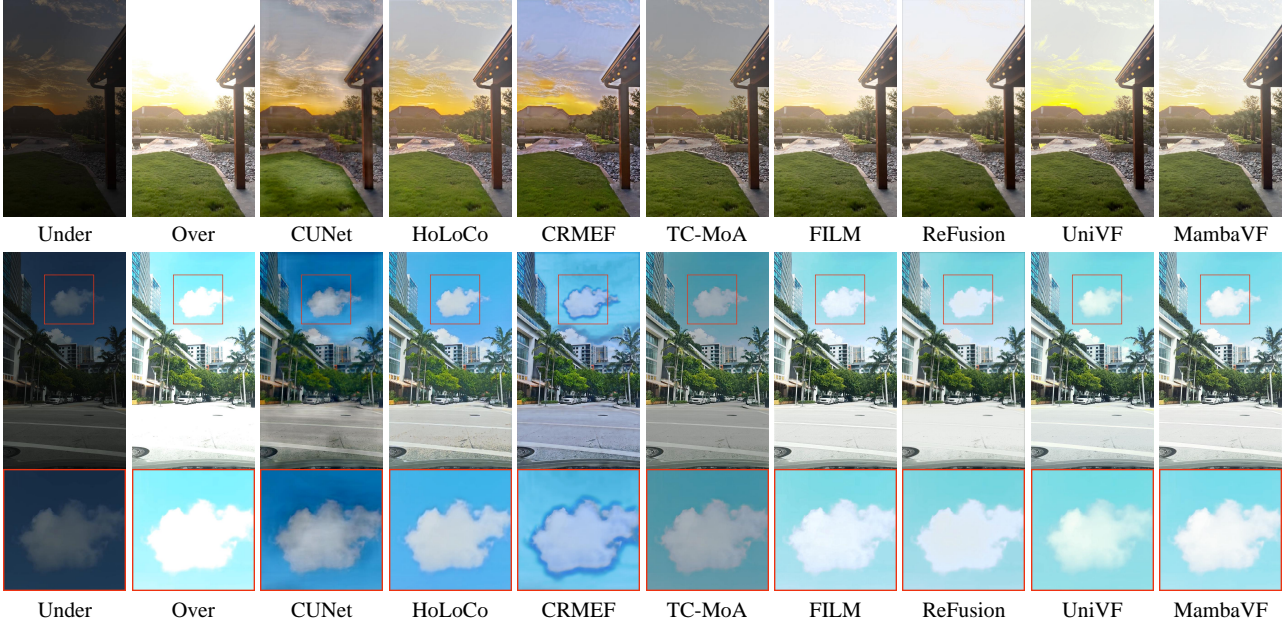


Figure 4. Visual comparison of fused results on multi-exposure video fusion.

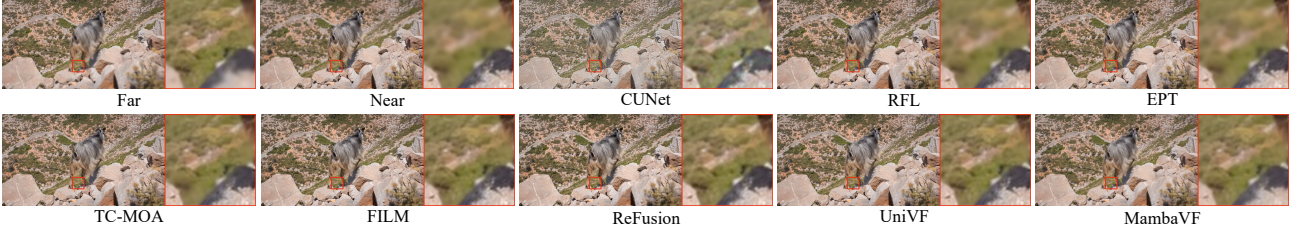


Figure 5. Visual comparison of fused results on multi-focus video fusion.

4.3. Efficiency Analysis

A cornerstone of the MambaVF framework is its superior computational efficiency, which is particularly vital for real-time video processing. To quantify this advantage, we conduct a comprehensive comparison of computational overhead among MambaVF, the unified video fusion framework UniVF (Zhao et al., 2025), and the infrared-visible-specific video fusion model TemCoCo (Gong et al., 2025). We evaluate three critical metrics: the total number of parameters, FLOPs, and average inference latency.

As detailed in Fig. 1 and Tab. 5, MambaVF exhibits a remarkably lean architecture. Compared to the leading flow-based baseline UniVF, our model requires only **7.75%** of the parameters and **11.21%** of the FLOPs. This drastic reduction in computational footprint stems primarily from our flow-free design, which bypasses the heavy resource requirements of motion estimation and feature warping modules. Furthermore, MambaVF achieves a **2.1x** speedup in inference time over UniVF, significantly enhancing its real-time throughput. Our framework also demonstrates a clear

lead in efficiency when compared to TemCoCo, maintaining lower complexity while providing competitive fusion quality. These results underscore that the state-space-based paradigm is exceptionally well-suited for high-resolution video applications and deployment on hardware with limited computational budgets.

4.4. Ablation Studies

To further investigate the impact of our design choices, we conduct several controlled experiments on the MEF task in Tab. 4.

Architectural Components. We first analyze the effectiveness of the proposed Spatio-Temporal Bidirectional (STB) scanning strategy by comparing our 8-way traversal against two restricted baselines:

- (1) Exp. I: Substituting STB scanning with a standard 4-way 2D spatial scan.
- (2) Exp. II: Utilizing a simplified 1D temporal-only scan in place of STB scanning.

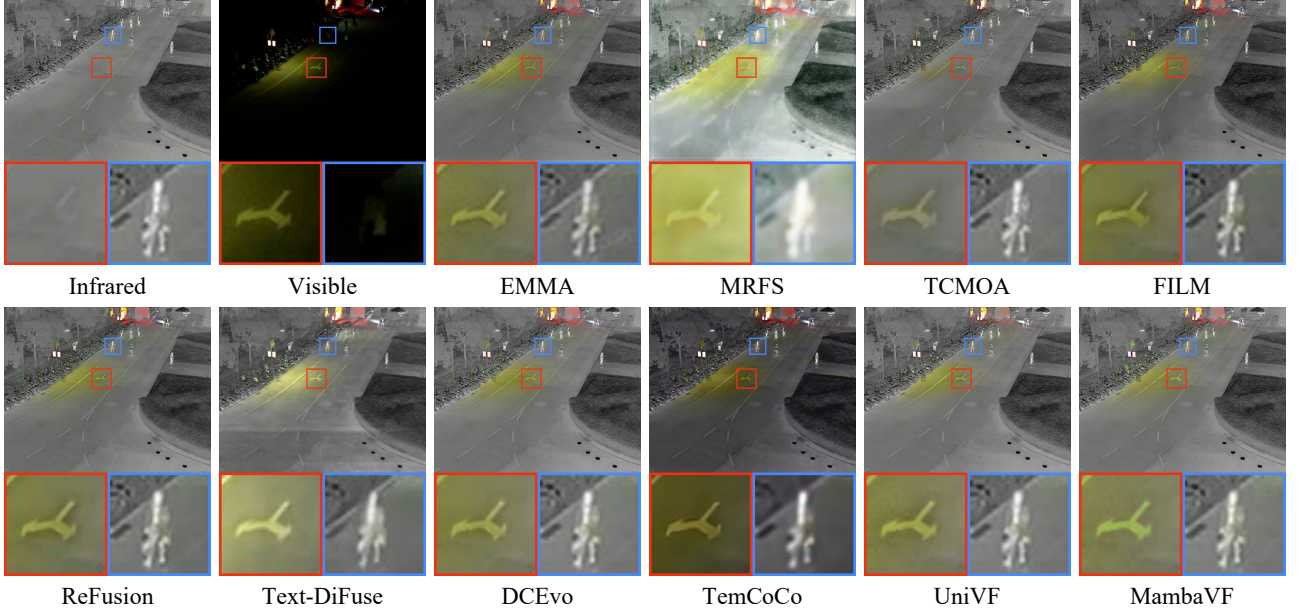


Figure 6. Visual comparison of fused results on infrared-visible video fusion.

Table 1. Quantitative evaluation results for the low-resolution MEF and MFF task. The **red** and **blue** highlights indicate the highest and second-highest scores.

| VF-Bench Multi-Exposure Fusion Branch (540p) | | | | | | VF-Bench Multi-Focus Fusion Branch (480p) | | | | | | | |
|--|-------------|-------------|-------------|-------------|-------------|---|---------|-------------|-------------|-------------|-------------|-------------|-------------|
| | VIF↑ | SSIM↑ | MI↑ | Qabf↑ | BiSWE↓ | MS2R↓ | | VIF↑ | SSIM↑ | MI↑ | Qabf↑ | BiSWE↓ | MS2R↓ |
| CUNet | 0.50 | 0.85 | 1.85 | 0.39 | 7.55 | 0.20 | CUNet | 0.53 | 0.86 | 3.52 | 0.68 | 10.23 | 0.42 |
| HoLoCo | 0.50 | 0.86 | 2.56 | 0.42 | 8.22 | 0.19 | RFL | 0.77 | 0.90 | 6.31 | 0.78 | 8.46 | 0.28 |
| CRMEF | 0.62 | 0.94 | 2.60 | 0.63 | 8.72 | 0.19 | EPT | 0.76 | 0.90 | 6.33 | 0.78 | 8.50 | 0.29 |
| TC-MoA | 0.74 | 0.99 | 2.93 | 0.72 | 7.82 | 0.16 | TC-MoA | 0.75 | 0.90 | 5.27 | 0.77 | 8.39 | 0.28 |
| FILM | 0.77 | 0.99 | 4.35 | 0.72 | 8.28 | 0.17 | FILM | 0.75 | 0.89 | 5.06 | 0.78 | 8.61 | 0.33 |
| ReFus | 0.74 | 0.97 | 3.81 | 0.72 | 7.63 | 0.16 | ReFus | 0.73 | 0.90 | 4.93 | 0.77 | 8.00 | 0.32 |
| UniVF | 0.79 | 0.99 | 4.38 | 0.73 | 6.96 | 0.16 | UniVF | 0.77 | 0.90 | 6.34 | 0.79 | 8.29 | 0.27 |
| MambaVF | 0.82 | 0.99 | 4.40 | 0.75 | 7.37 | 0.15 | MambaVF | 0.75 | 0.92 | 5.37 | 0.80 | 7.53 | 0.27 |

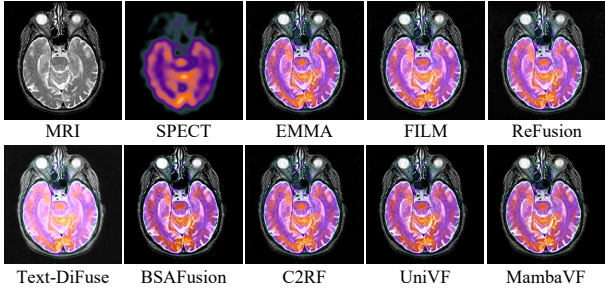


Figure 7. Visual comparison of fused results on MVF.

The quantitative results reveal that the 2D spatial scan is insufficient for video-level tasks, as it fails to model inter-frame dependencies, resulting in elevated BiSWE values and visible flickering. Conversely, the 1D temporal scan captures motion but neglects fine-grained spatial textures,

leading to a degradation in structural metrics. Our 8-way STB scanning achieves the optimal equilibrium by traversing the video cube from multiple perspectives, effectively capturing both the evolution of individual pixels and complex intra-frame geometries.

Temporal Context and Decoder Refinement. We further investigate the impact of temporal depth and local refinement modules through two additional configurations:

(3) Exp. III: Restricting the model to a single-frame input, effectively degrading MambaVF into a conventional frame-by-frame image fusion model.

(4) Exp. IV: Replacing the 2D ResBlocks in Decoder with their 3D counterparts to evaluate the necessity of additional volumetric processing during the reconstruction phase.

The transition from multi-frame to single-frame input (Exp. III) caused a substantial drop in overall fusion quality, un-

Table 2. Quantitative evaluation for the IVF task.

| VF-Bench Infrared-Visible Video Fusion Branch | | | | | | |
|---|-------|--------|------|--------|---------|--------|
| | VIF ↑ | SSIM ↑ | MI ↑ | Qabf ↑ | BiSWE ↓ | MS2R ↓ |
| EMMA | 0.37 | 0.63 | 2.01 | 0.58 | 4.79 | 0.37 |
| TC-MoA | 0.37 | 0.64 | 2.05 | 0.60 | 4.68 | 0.38 |
| MRFS | 0.27 | 0.55 | 1.48 | 0.34 | 6.09 | 0.38 |
| FILM | 0.40 | 0.63 | 2.05 | 0.64 | 4.78 | 0.37 |
| ReFus | 0.42 | 0.64 | 2.27 | 0.67 | 4.64 | 0.36 |
| Text-D | 0.30 | 0.60 | 1.64 | 0.39 | 10.63 | 0.40 |
| DCEvo | 0.43 | 0.64 | 2.44 | 0.66 | 4.57 | 0.37 |
| TemCoCo | 0.29 | 0.60 | 1.77 | 0.41 | 4.66 | 0.46 |
| UniVF | 0.44 | 0.64 | 2.47 | 0.68 | 3.94 | 0.35 |
| MambaVF | 0.44 | 0.65 | 2.40 | 0.68 | 3.91 | 0.36 |

Table 3. Quantitative evaluation for the MVF task.

| VF-Bench Medical Video Fusion Branch | | | | | | |
|--------------------------------------|-------|--------|------|--------|---------|--------|
| | VIF ↑ | SSIM ↑ | MI ↑ | Qabf ↑ | BiSWE ↓ | MS2R ↓ |
| EMMA | 0.29 | 0.68 | 1.73 | 0.60 | 30.00 | 1.98 |
| FILM | 0.33 | 0.36 | 1.83 | 0.67 | 32.04 | 1.59 |
| ReFus | 0.31 | 0.32 | 1.74 | 0.67 | 32.85 | 1.74 |
| Text-D | 0.24 | 0.21 | 1.58 | 0.52 | 34.09 | 1.96 |
| BSAF | 0.28 | 0.63 | 1.69 | 0.58 | 34.73 | 1.66 |
| C2RF | 0.30 | 0.73 | 1.75 | 0.59 | 32.67 | 2.06 |
| UniVF | 0.35 | 0.76 | 2.00 | 0.68 | 29.61 | 1.30 |
| MambaVF | 0.36 | 0.76 | 2.00 | 0.68 | 29.61 | 1.27 |

Table 4. Results of the ablation experiments, with the best-performing values highlighted in red.

| Descriptions | Configurations | | | Metrics | | | | | |
|---------------------------|----------------|------------|--------------|---------|--------|------|--------|---------|--------|
| | scan type | 3D decoder | multi-inputs | VIF ↑ | SSIM ↑ | MI ↑ | Qabf ↑ | BiSWE ↓ | MS2R ↓ |
| Exp. I: 2D spatial scan | 2D | ✗ | ✓ | 0.72 | 0.95 | 2.89 | 0.65 | 8.43 | 0.19 |
| Exp. II: 1D temporal scan | 1D | ✗ | ✓ | 0.63 | 0.93 | 2.67 | 0.61 | 8.68 | 0.18 |
| Exp. III: Multi-inputs | 2D | ✗ | ✗ | 0.68 | 0.94 | 2.75 | 0.64 | 8.89 | 0.19 |
| Exp. IV: Decoder | 3D | ✓ | ✓ | 0.79 | 0.99 | 4.38 | 0.73 | 7.59 | 0.16 |
| MambaVF (Ours) | 3D | ✗ | ✓ | 0.82 | 0.99 | 4.40 | 0.75 | 7.37 | 0.15 |

Table 5. Total number of parameters, FLOPs, and inference time Comparison between TemCoCo (Gong et al., 2025), UniVF (Zhao et al., 2025) and our MambaVF.

| Methods | Params (M) | FLOPs (G) | Latency (ms) |
|---------|------------|-----------|--------------|
| TemCoCo | 19.21 | 147.05 | 18.32 |
| UniVF | 9.16 | 78.23 | 71.07 |
| MambaVF | 0.71 | 8.77 | 33.37 |

derscoring the necessity of temporal context for maintaining coherence in video fusion. Regarding the decoder architecture (Exp. IV), we observed that while 3D Residual Blocks aim to capture deeper spatio-temporal features, they actually yielded a slight performance decrease and introduced significant computational overhead. Adhering to the principle of parsimony (Occam’s Razor), we retain the 2D Residual Blocks, as they provide superior texture refinement with significantly lower resource consumption.

Impact of VSS Blocks and Hidden State Dimension. We analyze the sensitivity of MambaVF to the number of VSS blocks and the latent dimension in Fig. 8. Increasing the depth of the Mamba encoder improves the fusion performance but introduces additional latency. We found that a depth of 3 blocks provides an optimal trade-off for most real-time scenarios. Furthermore, increasing the latent dimension beyond 32 does not lead to significant performance gains, but it does increase computational cost. Therefore, we choose 3 VSS blocks with an embedding dimension of 32 as our configuration.

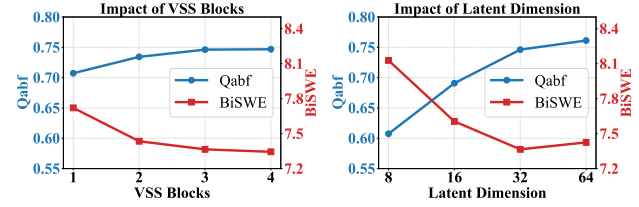


Figure 8. Hyperparameter analysis. The subplots illustrate the impact of the number of VSS Blocks (left) and Latent Dimension (right) on the model performance. The blue line represents Qabf (left axis), and the red line represents BiSWE (right axis).

5. Conclusion

In this paper, we introduced MambaVF, an efficient and flow-free framework for multi-source video fusion based on State Space Models. By shifting away from the traditional estimate-and-warp paradigm, we address the long-standing bottlenecks of computational redundancy and flow-dependency in video fusion. Our proposed Spatio-Temporal Bidirectional (STB) scanning mechanism allows for a comprehensive understanding of video content across spatial and temporal dimensions with linear complexity. Experimental results on the VF-Bench demonstrate that MambaVF not only achieves state-of-the-art performance across four major fusion tasks but also offers a significant reduction in parameters and runtime. We believe MambaVF provides a new, high-performance baseline for the deployment of video fusion algorithms on resource-constrained platforms and opens a promising direction for future research in efficient spatio-temporal modeling and fusion.

Impact Statement

This paper presents work whose goal is to advance the field of Machine Learning. There are many potential societal consequences of our work, none of which we feel must be specifically highlighted here.

References

Argaw, D. M., Liu, X., Chung, J. S., Liu, M.-Y., and Reda, F. Mambavideo for discrete video tokenization with channel-split quantization. *arXiv preprint arXiv:2507.04559*, 2025.

Bai, H., Zhang, J., Zhao, Z., Wu, Y., Deng, L., Cui, Y., Feng, T., and Xu, S. Task-driven image fusion with learnable fusion loss. In *IEEE Conf. Comput. Vis. Pattern Recog.*, pp. 7457–7468, 2025a.

Bai, H., Zhao, Z., Zhang, J., Jiang, B., Deng, L., Cui, Y., Xu, S., and Zhang, C. Deep unfolding multi-modal image fusion network via attribution analysis. *IEEE Trans. Circuit Syst. Video Technol.*, 35(4):3498–3511, 2025b.

Bai, H., Zhao, Z., Zhang, J., Wu, Y., Deng, L., Cui, Y., Jiang, B., and Xu, S. Refusion: Learning image fusion from reconstruction with learnable loss via meta-learning. *Int. J. Comput. Vis.*, 133(5):2547–2567, 2025c.

Bouzos, O., Andreadis, I., and Mitianoudis, N. A convolutional neural network-based conditional random field model for structured multi-focus image fusion robust to noise. *IEEE Trans. Image Process.*, 32:2915–2930, 2023.

Cao, Z., Zhong, Y., Wang, Z., and Deng, L.-J. Mmaif: Multi-task and multi-degradation all-in-one for image fusion with language guidance. In *Int. Conf. Comput. Vis.*, pp. 11744–11754, October 2025.

Chen, G., Huang, Y., Xu, J., Pei, B., Wang, J., Chen, Z., Li, Z., Lu, T., and Wang, L. Video mamba suite: State space model as a versatile alternative for video understanding. *Int. J. Comput. Vis.*, 134(1):20, 2026.

Chen, Z., Wang, Y., Cai, X., You, Z., Lu, Z., Zhang, F., Guo, S., and Xue, T. Ultrafusion: Ultra high dynamic imaging using exposure fusion. In *IEEE Conf. Comput. Vis. Pattern Recog.*, pp. 16111–16121, June 2025.

Cheng, C., Xu, T., Feng, Z., Wu, X., Tang, Z., Li, H., Zhang, Z., Ali, S. A., Awais, M., and Kittler, J. One model for ALL: low-level task interaction is a key to task-agnostic image fusion. In *IEEE Conf. Comput. Vis. Pattern Recog.*, pp. 28102–28112, 2025.

Deng, X. and Dragotti, P. L. Deep convolutional neural network for multi-modal image restoration and fusion. *IEEE Trans. Pattern Anal. Mach. Intell.*, 43(10):3333–3348, 2020.

Deng, X., Zhang, Y., Xu, M., Gu, S., and Duan, Y. Deep coupled feedback network for joint exposure fusion and image super-resolution. *IEEE Trans. Image Process.*, 30: 3098–3112, 2021.

Gao, F., Deng, X., Xu, M., Xu, J., and Dragotti, P. L. Multi-modal convolutional dictionary learning. *IEEE Trans. Image Process.*, 31:1325–1339, 2022.

Gong, M., Zhang, H., Yi, X., Tang, L., and Ma, J. Temoco: Temporally consistent multi-modal video fusion with visual-semantic collaboration. In *Int. Conf. Comput. Vis.*, pp. 14326–14335, 2025.

Gu, A. and Dao, T. Mamba: Linear-time sequence modeling with selective state spaces. In *Conf. on Language Modeling*, 2024.

Gu, A., Goel, K., and Ré, C. Efficiently modeling long sequences with structured state spaces. *arXiv preprint arXiv:2111.00396*, 2021.

Guan, Y., Xu, R., Yao, M., Wang, L., and Xiong, Z. Mutual-guided dynamic network for image fusion. In *ACM Int. Conf. Multimedia*, pp. 1779–1788, 2023.

Guo, H., Li, J., Dai, T., Ouyang, Z., Ren, X., and Xia, S.-T. Mambair: A simple baseline for image restoration with state-space model. In *Eur. Conf. Comput. Vis.*, pp. 222–241. Springer, 2024.

Han, D., Li, L., Guo, X., and Ma, J. Multi-exposure image fusion via deep perceptual enhancement. *Inf. Fusion*, 79: 248–262, 2022.

He, K., Zhang, X., Ren, S., and Sun, J. Deep residual learning for image recognition. In *IEEE Conf. Comput. Vis. Pattern Recog.*, pp. 770–778, 2016.

Jiang, Z., Zhang, Z., Fan, X., and Liu, R. Towards all weather and unobstructed multi-spectral image stitching: Algorithm and benchmark. In *ACM Int. Conf. Multimedia*, pp. 3783–3791, 2022.

Li, H. and Wu, X.-J. Densefuse: A fusion approach to infrared and visible images. *IEEE Trans. Image Process.*, 28(5):2614–2623, 2018.

Li, H., Xu, T., Wu, X., Lu, J., and Kittler, J. Lrrnet: A novel representation learning guided fusion network for infrared and visible images. *IEEE Trans. Pattern Anal. Mach. Intell.*, 45(9):11040–11052, 2023a.

Li, H., Zhang, Y., Zhu, J., Wang, S., Lee, M. A., Xu, H., Adelson, E., Fei-Fei, L., Gao, R., and Wu, J. See, hear, and feel: Smart sensory fusion for robotic manipulation. In *Conf. on Robot Learning*, pp. 1368–1378, 2023b.

Li, H., Su, D., Cai, Q., and Zhang, Y. Bsafusion: A bidirectional stepwise feature alignment network for unaligned medical image fusion. In *AAAI*, pp. 4725–4733, 2025.

Li, J., Liu, J., Zhou, S., Zhang, Q., and Kasabov, N. K. Gesenet: A general semantic-guided network with couple mask ensemble for medical image fusion. *IEEE Trans. Neural Networks Learn. Syst.*, pp. 1–14, 2023c.

Li, K., Li, X., Wang, Y., He, Y., Wang, Y., Wang, L., and Qiao, Y. Videomamba: State space model for efficient video understanding. In *Eur. Conf. Comput. Vis.*, pp. 237–255. Springer, 2024.

Liang, P., Jiang, J., Liu, X., and Ma, J. Fusion from decomposition: A self-supervised decomposition approach for image fusion. In *Eur. Conf. Comput. Vis.*, pp. 719–735, 2022.

Liu, J., Fan, X., Huang, Z., Wu, G., Liu, R., Zhong, W., and Luo, Z. Target-aware dual adversarial learning and a multi-scenario multi-modality benchmark to fuse infrared and visible for object detection. In *IEEE Conf. Comput. Vis. Pattern Recog.*, pp. 5792–5801, 2022.

Liu, J., Wu, G., Luan, J., Jiang, Z., Liu, R., and Fan, X. Holoco: Holistic and local contrastive learning network for multi-exposure image fusion. *Inf. Fusion*, 95:237–249, 2023.

Liu, J., Zhang, B., Mei, Q., Li, X., Zou, Y., Jiang, Z., Ma, L., Liu, R., and Fan, X. Dcevo: Discriminative cross-dimensional evolutionary learning for infrared and visible image fusion. In *IEEE Conf. Comput. Vis. Pattern Recog.*, pp. 2226–2235, 2025.

Liu, Y., Tian, Y., Zhao, Y., Yu, H., Xie, L., Wang, Y., Ye, Q., Jiao, J., and Liu, Y. Vmamba: Visual state space model. *Adv. Neural Inform. Process. Syst.*, 37:103031–103063, 2024a.

Liu, Z., Liu, J., Wu, G., Chen, Z., Fan, X., and Liu, R. Searching a compact architecture for robust multi-exposure image fusion. *IEEE Trans. Circuit Syst. Video Technol.*, 34(7):6224–6237, 2024b.

Ma, J., Yu, W., Liang, P., Li, C., and Jiang, J. Fusiongan: A generative adversarial network for infrared and visible image fusion. *Inf. Fusion*, 48:11–26, 2019.

Ma, J., Xu, H., Jiang, J., Mei, X., and Zhang, X. S. Ddcgan: A dual-discriminator conditional generative adversarial network for multi-resolution image fusion. *IEEE Trans. Image Process.*, 29:4980–4995, 2020.

Ma, K., Zeng, K., and Wang, Z. Perceptual quality assessment for multi-exposure image fusion. *IEEE Trans. Image Process.*, 24(11):3345–3356, 2015.

Prabhakar, K. R., Srikanth, V. S., and Babu, R. V. Deepfuse: A deep unsupervised approach for exposure fusion with extreme exposure image pairs. In *Int. Conf. Comput. Vis.*, pp. 4724–4732, 2017.

Prakash, A., Chitta, K., and Geiger, A. Multi-modal fusion transformer for end-to-end autonomous driving. In *IEEE Conf. Comput. Vis. Pattern Recog.*, pp. 7077–7087, 2021.

Qu, L., Liu, S., Wang, M., and Song, Z. Transmef: A transformer-based multi-exposure image fusion framework using self-supervised multi-task learning. In *AAAI*, pp. 2126–2134, 2022.

Ren, W., Ma, W., Yang, H., Wei, C., Zhang, G., and Chen, W. Vamba: Understanding hour-long videos with hybrid mamba-transformers. In *Int. Conf. Comput. Vis.*, pp. 21197–21208, October 2025.

Tang, L., Wang, Y., Gong, M., Li, Z., Deng, Y., Yi, X., Li, C., Xu, H., Zhang, H., and Ma, J. Videofusion: A spatio-temporal collaborative network for multi-modal video fusion and restoration. *arXiv preprint arXiv:2503.23359*, 2025a.

Tang, L., Yan, Q., Xinyu Xiang, L. F., and Ma, J. C2rf: Bridging multi-modal image registration and fusion via commonality mining and contrastive learning. *Int. J. Comput. Vis.*, 2025b.

Wang, D., Liu, J., Fan, X., and Liu, R. Unsupervised misaligned infrared and visible image fusion via cross-modality image generation and registration. In *IJCAI*, pp. 3508–3515, 2022a.

Wang, Z., Li, X., Duan, H., and Zhang, X. A self-supervised residual feature learning model for multifocus image fusion. *IEEE Trans. Image Process.*, 31:4527–4542, 2022b.

Wang, Z., Li, X., Zhao, L., Duan, H., Wang, S., Liu, H., and Zhang, X. When multi-focus image fusion networks meet traditional edge-preservation technology. *Int. J. Comput. Vis.*, 131(10):2529–2552, 2023.

Wang, Z., Zhang, J., Guan, T., Zhou, Y., Li, X., Dong, M., and Liu, J. Efficient rectified flow for image fusion. 2025.

Xie, H., Sang, M., Zhang, Y., Yang, Y., Zhao, S., and Zhong, J. Rcvf: A unified registration and fusion framework for video streams. *IEEE Trans. Multimedia*, 2024.

Xu, H., Ma, J., Jiang, J., Guo, X., and Ling, H. U2fusion: A unified unsupervised image fusion network. *IEEE Trans. Pattern Anal. Mach. Intell.*, 44(1):502–518, 2022a.

Xu, H., Ma, J., Yuan, J., Le, Z., and Liu, W. Rfnet: Unsupervised network for mutually reinforcing multi-modal image registration and fusion. In *IEEE Conf. Comput. Vis. Pattern Recog.*, pp. 19647–19656, 2022b.

Xu, S., Zhang, J., Zhao, Z., Sun, K., Liu, J., and Zhang, C. Deep gradient projection networks for pan-sharpening. In *IEEE Conf. Comput. Vis. Pattern Recog.*, pp. 1366–1375, 2021.

Yang, Y., Xing, Z., Yu, L., Fu, H., Huang, C., and Zhu, L. Vivim: A video vision mamba for ultrasound video segmentation. *IEEE Trans. Circuit Syst. Video Technol.*, 35(10):10293–10304, 2025.

Zhang, H., Cao, L., and Ma, J. Text-difuse: An interactive multi-modal image fusion framework based on text-modulated diffusion model. In *Adv. Neural Inform. Process. Syst.*, 2024a.

Zhang, H., Zuo, X., Jiang, J., Guo, C., and Ma, J. Mrfs: Mutually reinforcing image fusion and segmentation. In *IEEE Conf. Comput. Vis. Pattern Recog.*, pp. 26974–26983, 2024b.

Zhang, H., Cao, L., Zuo, X., Shao, Z., and Ma, J. Omnidfuse: Composite degradation-robust image fusion with language-driven semantics. *IEEE Trans. Pattern Anal. Mach. Intell.*, 47(9):7577–7595, 2025.

Zhang, X. Deep learning-based multi-focus image fusion: A survey and a comparative study. *IEEE Trans. Pattern Anal. Mach. Intell.*, 44(9):4819–4838, 2021.

Zhao, W., Xie, S., Zhao, F., He, Y., and Lu, H. Metafusion: Infrared and visible image fusion via meta-feature embedding from object detection. In *IEEE Conf. Comput. Vis. Pattern Recog.*, pp. 13955–13965. IEEE, 2023a.

Zhao, Z., Xu, S., Zhang, C., Liu, J., Zhang, J., and Li, P. DIDFuse: Deep image decomposition for infrared and visible image fusion. In *IJCAI*, pp. 970–976, 2020.

Zhao, Z., Xu, S., Zhang, J., Liang, C., Zhang, C., and Liu, J. Efficient and model-based infrared and visible image fusion via algorithm unrolling. *IEEE Transactions on Circuits and Systems for Video Technology*, 32(3):1186–1196, 2022a.

Zhao, Z., Zhang, J., Xu, S., Lin, Z., and Pfister, H. Discrete cosine transform network for guided depth map super-resolution. In *IEEE Conf. Comput. Vis. Pattern Recog.*, pp. 5687–5697, 2022b.

Zhao, Z., Bai, H., Zhang, J., Zhang, Y., Xu, S., Lin, Z., Timofte, R., and Van Gool, L. Cddfuse: Correlation-driven dual-branch feature decomposition for multi-modality image fusion. In *IEEE Conf. Comput. Vis. Pattern Recog.*, pp. 5906–5916, 2023b.

Zhao, Z., Bai, H., Zhu, Y., Zhang, J., Xu, S., Zhang, Y., Zhang, K., Meng, D., Timofte, R., and Van Gool, L. Ddfm: Denoising diffusion model for multi-modality image fusion. In *Int. Conf. Comput. Vis.*, pp. 8082–8093, 2023c.

Zhao, Z., Bai, H., Zhang, J., Zhang, Y., Zhang, K., Xu, S., Chen, D., Timofte, R., and Gool, L. V. Equivariant multi-modality image fusion. In *IEEE Conf. Comput. Vis. Pattern Recog.*, pp. 25912–25921. IEEE, 2024a.

Zhao, Z., Deng, L., Bai, H., Cui, Y., Zhang, Z., Zhang, Y., Qin, H., Chen, D., Zhang, J., Wang, P., and Gool, L. V. Image fusion via vision-language model. In *Int. Conf. Mach. Learn.*, 2024b.

Zhao, Z., Bai, H., Ke, B., Cui, Y., Deng, L., Zhang, Y., Zhang, K., and Schindler, K. A unified solution to video fusion: From multi-frame learning to benchmarking. In *Adv. Neural Inform. Process. Syst.*, 2025.

Zhong, H., Tang, F., Chen, Z., Chang, H. J., and Gao, Y. Amdanet: Attention-driven multi-perspective discrepancy alignment for rgb-infrared image fusion and segmentation. In *Int. Conf. Comput. Vis.*, pp. 10645–10655, October 2025.

Zhu, L., Liao, B., Zhang, Q., Wang, X., Liu, W., and Wang, X. Vision mamba: Efficient visual representation learning with bidirectional state space model. *arXiv preprint arXiv:2401.09417*, 2024a.

Zhu, P., Sun, Y., Cao, B., and Hu, Q. Task-customized mixture of adapters for general image fusion. In *IEEE Conf. Comput. Vis. Pattern Recog.*, pp. 7099–7108. IEEE, 2024b.

A. Additional Qualitative Fusion Comparison Results

Additional visual evidence is provided in the figures below to further demonstrate the performance of our framework:

- Further visual results for the *Multi-exposure Video Fusion* task are presented in Fig. 9.
- Further visual results for the *Multi-focus Video Fusion* task are presented in Fig. 10.
- Further visual results for the *Infrared-Visible Video Fusion* task are presented in Fig. 11.
- Further visual results for the *Medical Video Fusion* task are presented in Fig. 12.

These visual evaluations corroborate our primary findings: MambaVF faithfully recovers subtle structures and intricate textures from source inputs while successfully merging complementary features into high-quality, information-rich fused frames. Furthermore, the video sequences included in the supplementary materials highlight the robust temporal stability of our method, characterized by a significant reduction in inter-frame jitter and motion artifacts.

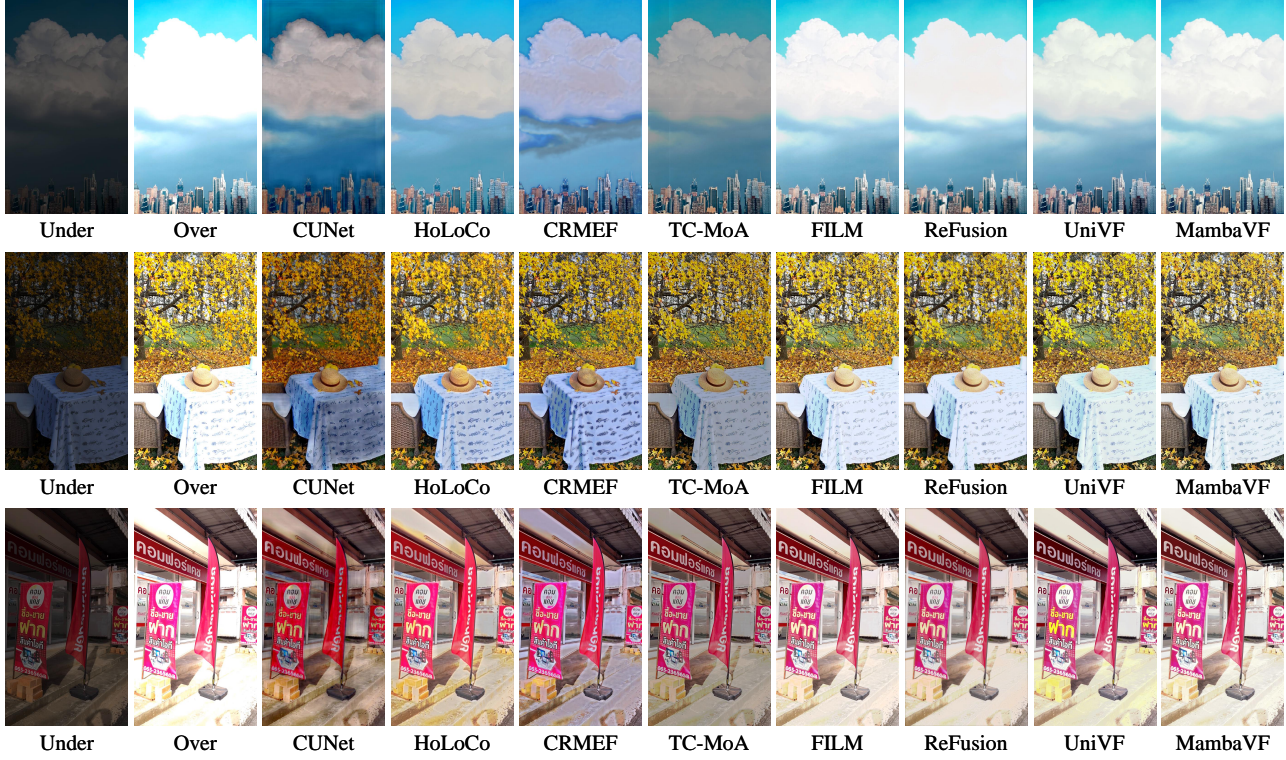


Figure 9. Visual comparison of fused results on multi-exposure video fusion.

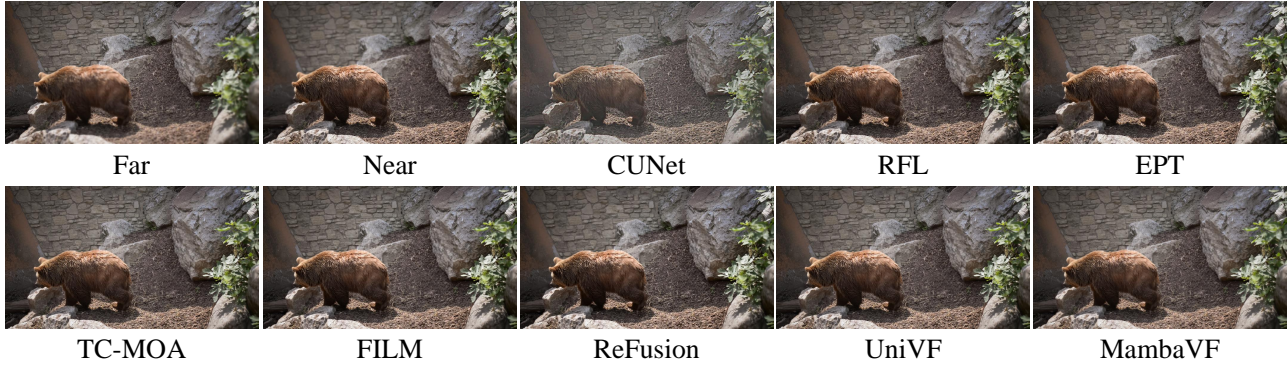


Figure 10. Visual comparison of fused results on multi-focus video fusion.

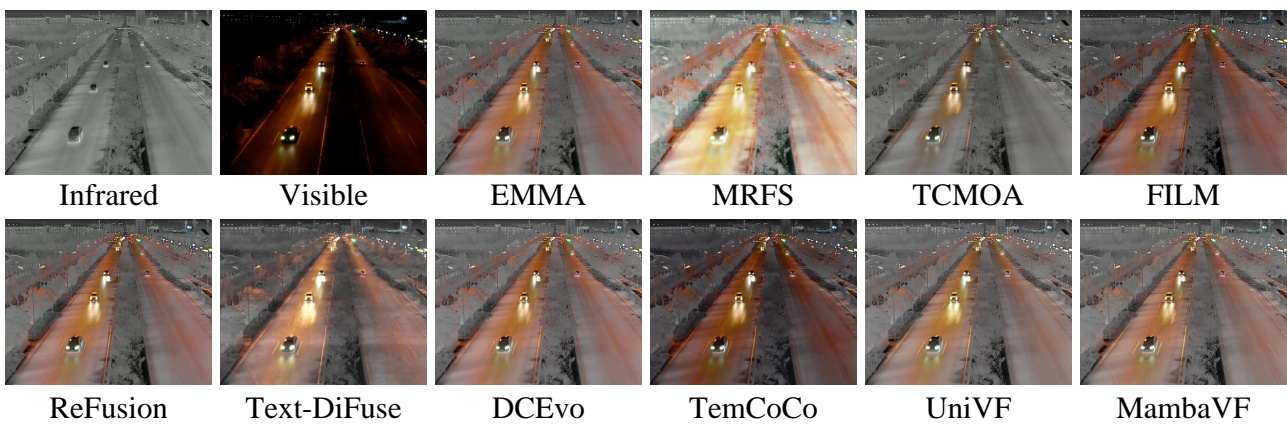


Figure 11. Visual comparison of fused results on infrared-visible video fusion.

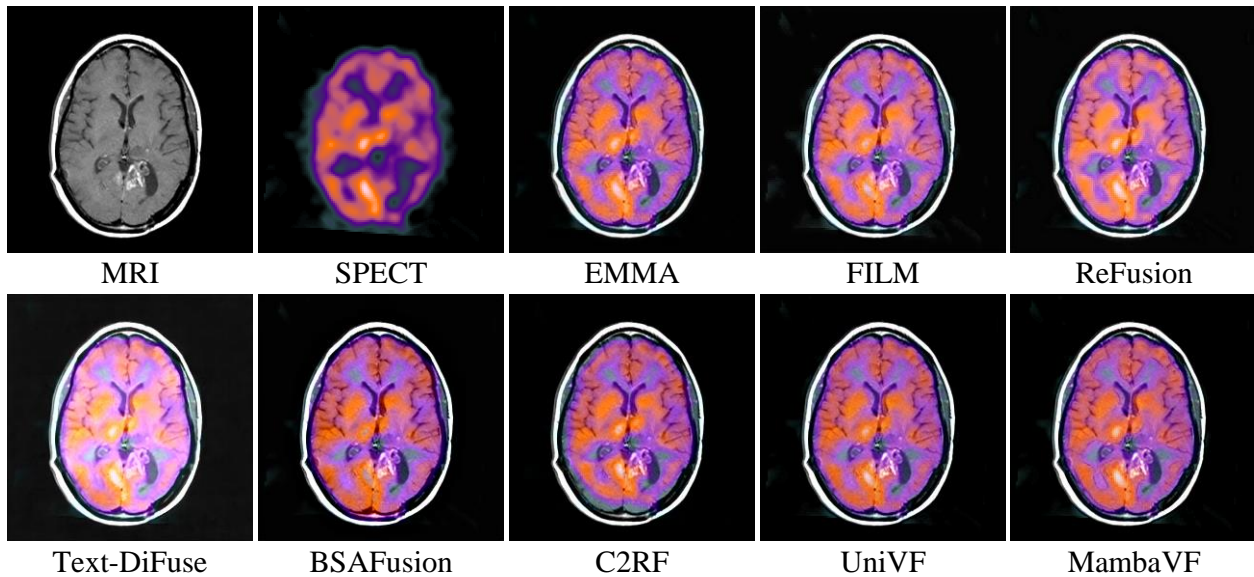


Figure 12. Visual comparison of fused results on medical video fusion.